A Novel Nucleus-Based Classifier for Discrimination of Osteoclasts and Mesenchymal Precursor Cells in Mouse Bone Marrow Cultures

Andreas Heindl, Alexander K. Seewald, Martin Schepelmann, Radu Rogojanu, Giovanna Bises, Theresia Thalhammer, and Isabella Ellinger

Abstract—Bone remodeling occurs by the balanced action of bone resorbing osteoclasts (OC) and bone-building osteoblasts. Increased bone resorption by excessive OC activity contributes to malignant and non-malignant diseases including osteoporosis. To study OC differentiation and function, OC formed in in vitro cultures are currently counted manually, a tedious procedure which is prone to inter-observer differences. Aiming for an automated OC-quantification system, classification of OC and precursor cells was done on fluorescence microscope images based on the distinct appearance of fluorescent nuclei. Following ellipse fitting to nuclei, a combination of eight features enabled clustering of OC and precursor cell nuclei. After evaluating different machine-learning techniques, LO-GREG achieved 74% correctly classified OC and precursor cell nuclei, outperforming human experts (best expert: 55%). In combination with the automated detection of total cell areas, this system allows to measure various cell parameters and most importantly to quantify proteins involved in osteoclastogenesis.

Keywords—osteoclasts, machine learning, ellipse fitting.

I. INTRODUCTION

BONE remodeling by the balanced action of mult-inucleated bone resorbing cells (osteoclasts, OC) and subsequent formation of bone mass by bone-building osteoblasts is important for maintaining bone mass and strength as well as mineral homeostasis in the human body [1], [2]. Excessive osteoclast activity leads to increased bone resorption causing local and systemic osteopenia as observed in diseases like osteoporosis and rheumatoid arthritis as well as in primary and secondary malignancies of the bone (osteosarcoma, bone metastasis; [3], [4]). Therefore, excess bone resorption by OC is a major research issue and focus of therapeutic invention in bone-related diseases [5]. In vitro cultures of OC allow for analysis of parameters and substances that stimulate or inhibit OC formation by differentiation and fusion from isolated mesenchymal precursor cells and can further

A. Heindl is with the Department of Pathophysiology and Allergy Research, Center for Pathophysiology, Infectiology and Immunology, Medical University of Vienna and Seewald Solutions, Vienna, Austria.

G. Bises, T. Thalhammer and I. Ellinger are with the Department of Pathophysiology and Allergy Research, Center for Pathophysiology, Infectiology and Immunology, Medical University of Vienna, Austria.

AK. Seewald is with Seewald Solutions, Vienna, Austria. phone: +43-664-1106886; e-mail: alex@seewald.at

R. Rogojanu is with Tissuegnostics GmbH, Vienna, Austria.

be used to analyze the effects of OC-targeted therapies [6]. Currently, the evaluation of OC formation in culture is based on the histochemical staining for tartrate-resistant alkaline phosphatase (TRAP), a protein highly expressed in mature OC, followed by manual counting of TRAP-positive, multinucleated ($\geq$ 3 nuclei) cells under the microscope [7], [8]. Although the histochemical staining procedure for TRAP is fast, the subsequent human identification of TRAP-positive OC on the slide is a time consuming task. In addition, the sometimes rather faint staining of the multinucleated cells and the lack of orientation on the coverslip make the counting of OCs in culture often difficult and result in large inter- and intra-observer variability. The major disadvantage of the visual evaluation, however, is that determining other parameters such as the number of precursor cells, cell area, or number of nuclei/OC is not in the least feasible. Due to the histochemical procedure, the specific detection (and quantification) of additional proteins or molecules by a subsequent staining procedure in OC and precursor cells is no longer possible. As the expression patterns of targets may differ in precursor cells and OC, assessment of cellular levels of these targets after pharmacological treatments can reveal important information for the understanding of the physiology and pathology of bone resorbing processes. Immunofluorescence (IF) microscopy allows parallel detection of several molecules within the same experiment, given that differentially labeled fluorescence-conjugated antibodies or probes are applied and detected by a fluorescence microscope at their respective excitation/emission wavelengths [9]. We have previously developed an automated method for OC and precursor cell detection [10]. In this setting, cell detection and the subsequent OC and precursor cell discrimination require three different staining steps. Although staining for additional proteins could be performed, only microscopes equipped with four or more different fluorescence filters/channels are suitable for the further evaluation of protein patterns of interest. Additionally, staining protocols with four or more different target proteins are complex to create and execute. To overcome these difficulties, we searched for other criteria to discriminate between OC and precursor cells. Indeed, changes of the shape and appearance of nuclei in the course of development of cells are well known (e.g. [11]–[13]) and may also be applicable to identify OCs in cell culture. The

human observer may be able to identify/describe these differences such as varying nuclei size, which would then allow for developing algorithms that are specifically based on these criteria [14]. Alternatively, unknown differences among nuclei of different cell populations may be unveiled by the aid of advanced microscopic or computer technologies [15]. We have developed an automated system, which uses shape and texture features of nuclei and machine learning algorithms for the classification of OC and their mesenchymal precursor cell nuclei. Training, validation and application of the classifier are described.

II. Materials and Methods

IF-labeling protocol for generation of ground truth data: The culture conditions to generate isolated murine OC and the IF-staining protocol required for cell detection and classification of OC and precursor cells based on amount of nuclei (DAPI staining) and F4/80 macrophage marker expression has been described in detail in [10]. In brief, mouse bone marrow cells were collected in minimum essential medium and plated in 24-well plates, each well containing a glass cover slip. OC formation from precursor cells was stimulated by incubation of the cells for 8 days in medium containing 25 ng / ml receptor activator of nuclear factor B ligand (RANKL) and 15 ng / ml macrophage colony stimulating factor (M-CSF). The cells were fixed and all cells were stained using two antibodies: one directed against the calcitonin receptor (Acris, Herford, Germany), staining the border of cells, and another one directed against α-tubulin (SigmaAldrich, Deisenhofen, Germany), staining cytoskeletal elements. Both antibodies were visualized using an Alexa Fluor 647-conjugated secondary antibody (Invitrogen, Carlsbad, CA, USA). This staining step is necessary to identify total areas of all cells. For discrimination of OC from precursor an antibody directed against F4/80 macrophage marker (eBioscience, San Diego, CA, USA) was applied, which is expressed predominantly in precursor cells, and which was visualized with an Alexa Fluor 568-conjugated secondary antibody (Invitrogen). 4',6-diamidino-2-phenylindole (DAPI) staining was used to identify the nuclei. Finally, the coverslips with the fluorescence-labeled cells were mounted on slides and subjected to IF microscopy. Images of the stained cells were acquired in the fluorescence-channels corresponding to the applied fluorochromes using the TissueFAXS automated epi-fluorescence microscope (TissueGnostics GmbH, Vienna, Austria) with a 40x (oil) / NA 1.3 objective. To ensure correct focus, all images, were automatically taken on seven different heights of the microscope stage (2 m steps) and merged into one critically sharp image. IF-labeling protocol for cell area detection and nuclei-based classification: Staining for F4/80 macrophage marker in combination with the Alexa Fluor 568-conjugated secondary antibody is omitted. All other steps were the same.

III. Results

A. Generation of Ground Truth Data

Ground truth data from nuclei of OC and precursor cells in culture were generated on IF-images by five human experts trained in cell biology. The experts studied images from three fluorescence channels: the channel detecting Alexa Fluor 647-emitted fluorescence, where all cells are visible due to staining of cytoskeletal and membrane proteins (Fig. 1A), the channel detecting Alexa Fluor 568-emitted fluorescence, where the macrophage marker F4/80 labels predominantly the precursor cells (Fig. 1B) and the channel detecting DAPI-emitted fluorescence (DAPI-channel) for nuclei identification (Fig. 1C). In combination, these images enabled the experts to identify OC based on the criteria of multinuclearity (three or more nuclei/OC, Fig. 1C, asterisk) and low F4/80 staining intensity in OC (Fig. 1B, asterisk). Each expert independently identified OC. Cells identified by at least two experts were regarded as true OC. All other cells were regarded as precursor cells (ground truth data set 1 = GT1). Experts manually marked up the perimeter of the nuclei in the corresponding DAPI channel (Fig. 1D) using a Wacom Graphics Tablet and the image processing program Adobe Photoshop CS 4.0. A total number of 4293 perimeters were extracted (for examples see Fig. 1E) and served as ground truth data set 2 (= GT2).
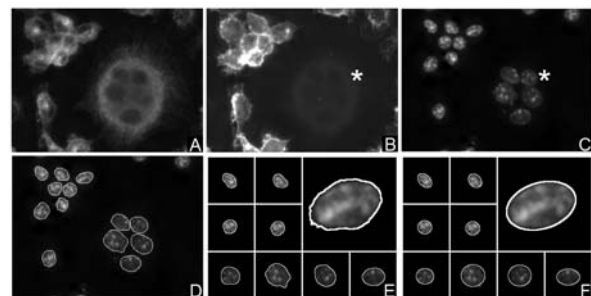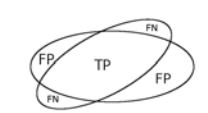

Fig. 1. IF microscopic images from cell cultures containing OC and their precursor cells were shown to human experts. Using the combined information from the images shown in (A), (B) and (C), the human experts classified the cell type (asterisk indicates an OC, ground truth data set 1) and marked up the nuclei (D; n = 4293). These manually drawn perimeters made up the ground truth data set 2 (E). Ellipse-fitting to these nuclei is shown in (F).

B. Application and Validation of an Ellipsoid-based Approach to Discriminate Cell Nuclei

For automated processing, the images derived from the DAPI-channel were binarized by adaptive thresholding [16] resulting in images where all nuclei have pixel values greater than zero. Boundary detection methods were applied to get the corresponding perimeter. The predominant elliptical shape of mammalian cell nuclei can be approximated by ellipse-fitting [17]. Therefore, we also fit ellipses using the least squares criterion (Fig. 1F) to obtain a geometrical figure that allows for subsequent investigation of shape and textural features computed

		Mean F1	Stdev
	Exp vs Exp	89.95	10.01
	Classifier vs Exp	85.79	13.62

	MLP	SVM	LOGREG
Training set S1, Test set S2	63.31	68.43	76.06
Training set S2, Test set S1	79.49	66.51	72.02
Mean	71.40	67.47	74.04

from perimeter and area covered by each nucleus and for discrimination between nuclei of OC and precursor cells thereafter. From these ellipses, the following set of eight features was derived: five texture-based features (mean value, standard deviation, kurtosis, entropy and skewness of intensities) and three shape-based features (length of axes a and b, times 2, area and eccentricity of the ellipse).

To assure that ellipses were suitable to model nuclei, we performed the following evaluation based on a pixel-wise comparison of areas: First, we compared the areas obtained by filling of marked perimeters (Fig. 1E, GT2) derived from individual human experts. In table I, this comparison is graphically exemplified. Pixels lying within both human expert markups are true positives (TP), pixels obtained from one expert only are either false positives (FP) or considered false negatives (FN). We computed the balanced F1-score [18],

$$F = 2 * \frac{precision * recall}{precision + recall} \quad (1)$$

$$precision = \frac{tn}{tn + tp} \quad (2)$$

$$recall = \frac{tp}{tp + tn} \quad (3)$$

, which is a weighted average of precision and recall for the areal agreement between individual human experts as shown in Table I. Subsequently, we compared the area of the fitted ellipse (Fig. 1F) for each nuclei in a pixel-wise manner with the area obtained from markups of individual expert. As shown in Table I, the overlapping confidence intervals of the computed F1-scores, suggest that description of nuclei by individual human experts and fitted ellipses is statistically indistinguishable.

We analyzed the set of features computed from the ellipses for their ability to discriminate OC and precursor nuclei. None of the single ellipse features enabled grouping of the two classes of nuclei, therefore we combined all features to enable discrimination. Sammon Mapping, a multidimensional scaling technique illustrates the eight dimensional space spanned by the calculated features [19]. Sammon Mapping optimizes a stress value that tries to preserve the inter-point distances of the n-dimensional feature space into the lower-dimensional projection space by Monte Carlo optimization. The result of this projection is depicted in Fig. 2. OC nuclei are represented by black dots whereas precursor cells are shown as grey crosses. The output of Sammon Mapping indicates two clusters of nuclei and suggests that OC and precursor cell nuclei can be distinguished by the features. This encouraged us to

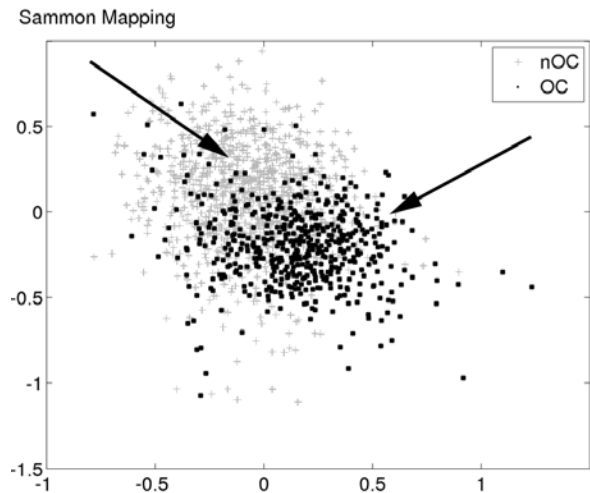train a machine-learning system in order to classify the nuclei.

Fig. 2. Sammon Mapping of all ellipse features of OC and precursor nuclei suggests that a combination of all features allows to distinguish between nuclei of OC (black dots) and precursor cells (grey crosses). The arrows indicate the centers of the clusters. Values shown on x- and y-axis are arbitrary as Sammon Mapping preserves only distances.

C. Training and Evaluation of a Machine-learning System for Discrimination of Nuclei of OC and Precursor Cells

Three machine-learning techniques were evaluated such as Multilayer Perceptron (MLP), Support Vector Machines (SVM) and Logistic Regression (LOGREG). We used the implementation shipped with Weka 3.6.5 [20]. The classifier was trained using two sets of nuclei: The first set (S1) consisted of 1307 OC-nuclei and the same amount of precursor cell nuclei. The second set (S2) contained 813 OC-nuclei and 866 precursor cell nuclei. Both sets S1 and S2 were used as training and as test set for the machine learning techniques (i.e. train by S1 and test by S2, and train by S2 and test by S1). The numbers of correctly classified nuclei (in comparison to GT1) are shown in Table 2. For each classifier, the corresponding mean from both resulting models was computed. Among the machine-learning techniques, LOGREG performed best with a mean of 74% correctly classified nuclei.

1) Performance and Application of the Nuclei-classifier: Having built the classifier, we were interested in comparing human and algorithm performance on an equalized level. Therefore, cell context information (shown e.g. in Fig. 1A-C) was removed and two human experts independently

classified extracted nuclei (n=84) as illustrated in Fig. 3A. This independent test set was created with a ratio of 50% OC and 50% precursor cell nuclei, which were randomly chosen from GT1. Due to the huge amount of marked up nuclei (n = 4293) it was very unlikely that one of the human experts would recognize the nuclei seen before during the ground truth creation process. LOGREG also performed best on this test set. The output of this evaluation is illustrated in Fig. 3B. LOGREG achieved a performance of 76% correctly classified nuclei whereas the best human expert only achieved a performance of about 55%. When only looking at nuclei where both experts agreed on the identity of the nuclei class the human performance decreased to only 30%.
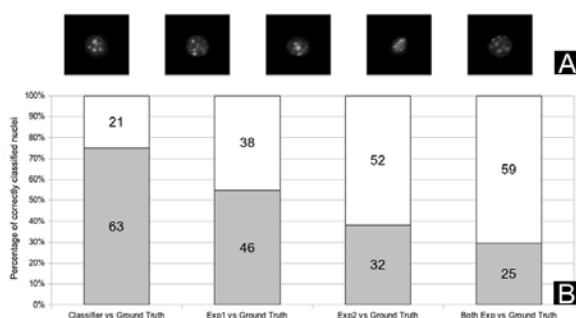

Fig. 3. Examples from the independent test set of nuclei, n= 84 (A). Evaluation of algorithm and human expert performance on the independent test set of nuclei (B). Numbers for correctly classified nuclei are shown in grey while numbers for incorrectly classified nuclei are shown in white.

The application of this classifier on virtual images derived from an in vitro culture of isolated murine OC is demonstrated in Fig. 4. From the images depicting the nuclei stained by DAPI (Fig. 4A), a binary mask is derived that shows nuclei in grey and background in black (Fig. 4B). Afterwards, ellipse-boundaries are detected (B, white lines) to enable ellipse fitting. Then the classifier can be used to divide the nuclei in two populations, namely OC-associated (Fig. 4C) or precursor cell-associated (Fig. 4D) nuclei. Incomplete nuclei at image borders cannot be classified. If, in addition to DAPI-staining, the entire cells were identified via IF-labeling of α-tubulin and calcitonin receptor (Fig. 4C and D) as outlined in material and methods [10], the classification of nuclei would enable cell classification (OC, precursor cells) and subsequent computing of cell-associated parameters of interest (area, shape, . . .). This combination of entire cell-staining and nuclei-staining via DAPI requires two fluorescence channels of a microscope, the usually available third fluorescence channel of the microscope remains free for investigation of a protein/molecule of interest that is to be quantitated in OC or precursor cells. Fig. 5A depicts OC-culture images (two fields of view), where total cell staining (α-tubulin and calcitonin receptor) and nuclear staining (DAPI) are combined. Application of the classifier to the DAPI channel of these images allows discrimination of two nuclei populations, namely OC-nuclei (Fig. 5B)

TABLE III
EXAMPLE RESULTS

	OC	Precursor cell
Number of cells	10	546
Total area of cells (pixel)	130466	548967
Mean area of cell (pixel)	13037	1003
Mean int. of F4/80 protein	29	51

and precursor cell-nuclei (Fig. 5C). The final combination of the cellular mask derived from Fig. 5A (according to [10]) with the classification accomplished in Fig. 5B and 5C enables the quantification of the expression level (fluorescence intensity) of any protein as well as other cell-associated parameters as exemplified in Table 3.
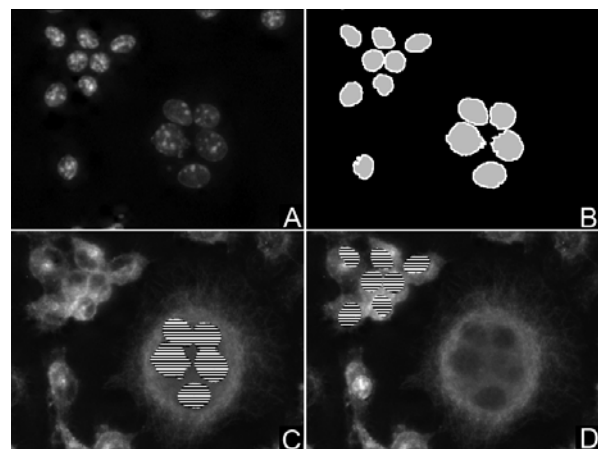

Fig. 4. IF microscopic images from cell cultures showing DAPI-stained nuclei of OC and their precursor cells (A). Binary mask of the same image showing nuclei in grey and background in black, including boundaries (white) (B) that are later used to inscribe ellipses. Nuclei-output of the classifier for OC(C) and precursor cells (D), both in black-white projected on the corresponding image showing α-tubulin/calcitonin-receptor stained total cell areas.

IV. DISCUSSION

To the best of our knowledge, this is the first time that ellipse fitting to nuclei has contributed to classify distinct bone cell types. Human experts observed that nuclei in OC are different from precursor cell nuclei, but could not describe the differences regarding their shape and texture. Nuclei are often elliptical in shape and there are recent examples that have used ellipse-detection algorithms for segmentation and separation of cell nuclei [21], [22]. Therefore, we validated the suitability of ellipses to describe nuclei-area, and illustrated the clustering of OC and precursor cell nuclei upon combination of eight shape- and texture- features of the ellipses by Sammon Mapping. Ellipse shape features alone were not sufficient for acceptable performance. Three machine-learning techniques (MLP, SVM and LOGREG) were tested as classifiers for the nuclei using these features. During the evaluation process performed on ground truth data obtained from human biological experts, the classifier LOGREG outperformed human experts in pure DAPI-based nuclei classification,
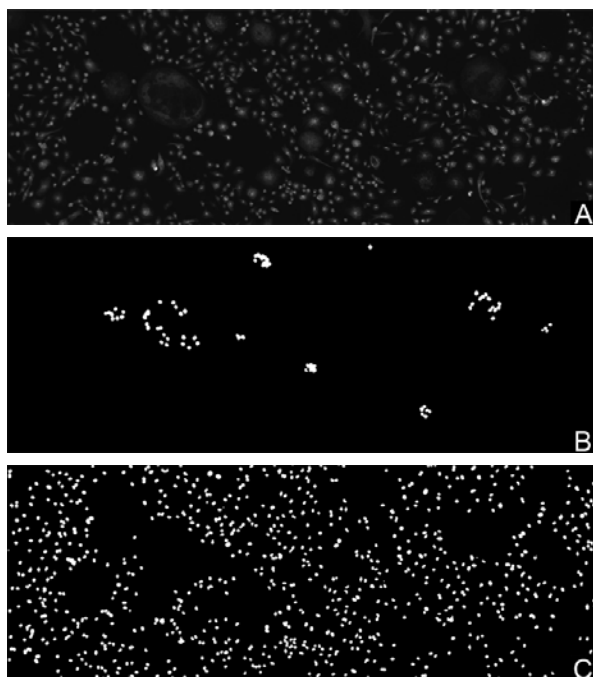
Fig. 5. IF microscopic images from OC-cell cultures showing -tubulin/calcitonin-receptor stained total cell areas in combination with DAPI-stained nuclei of OC and their precursor cells (A). Binary masks of the same image showing OC-nuclei (B) or precursor cell nuclei (C) in white after application of classifier (B).

where the best human expert only classified 55% of nuclei correctly and demonstrated correct classification of 74% of nuclei compared to GT1, where human experts had determined the cell type based on various cell parameters (amount of nuclei, protein markers expressed). A reproducible correct classification of 74% must be seen in relation to the observation that human experts, who are generally regarded as the golden standard exhibit intra- and interexpert variabilities in determination of OC and precursor cells. We determined a coefficient of variation of 30% among n=3 experts counting OC in the same region (unpublished observation) even when already compensating for systemic differences.

The existence of differences in the texture and shape of nuclei of various cell types, especially of tumor cells with variable prognostic factors [11]–[13] is well known. Indeed, histopathological assessment of the nuclear structure by brightfield microscopy remains the definitive clinical diagnostic approach to determine malignancy. In recent years, progress in the field of computerized 2D and even 3D image analysis was achieved, enabling quantification of nuclear morphology. This has been shown to be important for the assessment of the nuclear morphological changes associated with malignancy of tumors [15]. However, assignment of nuclei to different categories reflecting tumor grading is usually based on a priori knowledge of the criteria for nuclei-classification such as size, chromatin distribution, etc. This allows for specific adjustment of algorithm parameters [14]. Advanced tools such as 3D nuclear morphometry that help to depict unknown dif-

ferences between nuclei of different cell types are more time-intensive and therefore presumable not applicable for routine and high-throughput screening assays in osteoclast cultures [15]. The new classifier described herein requires solely the fluorescence-microscopic images acquired from the DAPI-labeled nuclei as input and rapidly returns the classification. The rapid staining procedure of cultured cells with DAPI (from fixation to embedding about one hour) and the fast performance of the classifier (few seconds for 5,000 nuclei) make the classifier ideally suited for large-scale screening assays. This new system has been developed to classify nuclei, which consequently will led to a better identification of different cell types. However, per se it is not able to identify and subsequently measure features of the nuclei-associated cells (e.g. cell-area, cell number). To achieve this, the classifier has to be combined with the IF-staining of a cytoskeletal protein (e.g. α-tubulin) found in every cell type, a protocol that requires about two more hours. Through the combination of an algorithm which is able to distinguish the cells from the background and the nuclei-discrimination system, many parameters of OC and precursor cells can be measured giving the system a significant improvement over the currently applied TRAP-staining and manual quantification of OC in cultures. Especially the possibility to quantify the expression levels of proteins in the target cells and determine protein up and down regulation during drug-treatment can open up new avenues in bone-disease related research. In summary, we developed a classifier which is suitable not only to quantitate OC in bone-marrow-derived cell cultures but additionally helps to determine precursor cell number and multiple cell-associated parameters.

V. Acknowledgments

References

[1] J. Edwards and G. Mundy, "Advances in osteoclast biology: old findings and new insights from mouse model," *Nat Rev Rheumatol.*, pp. 235–43, 2011.

[2] M. Bethel, E. Srour, and M. Kacena, "Hematopoietic cell regulation of osteoblast proliferation and differentiation," *Curr Osteoporos Rep.*, pp. 96–102, 2011.

[3] J. Edwards, M. Weivoda, and M. Kacena, "Osteoclasts: male-factors of disease and targets for treatment." *Discov Med.*, pp. 201–210, 2012.

[4] A. Ortiz, S. Lin, and M. Kacena, "Osteolytic and osteoblastic bone metastases: two extremes of the same spectrum?" *Recent Results Cancer Res.*, pp. 192–225, 2012.

[5] M. Broadhead, J. Clark, P. Choong, and D. Myers, "Therapeutic targeting of osteoclast function and pathways." *Expert Opin Ther Targets.*, pp. 169–181, 2011.

[6] E. Bradley and M. Oursler, "Osteoclast culture and resorption assays." *Methods MolBiol.*, pp. 19–35, 2008.

[7] G. Andersson and S. J. Marks, "Tartrate-resistant acid atpase as a cytochemical marker for osteoclasts." *J Histochem Cytochem.*, pp. 115–117, 1989.

[8] K. Henriksen, L. Tanko, P. Qvist, P. Delmas, C. Christiansen, and M. Karsdal, "Assessment of osteoclast number and function: application in the development of new and improved treatment modalities for bone diseases." *Osteoporos Int.*, pp. 681–685, 2007.

[9] T. Suzuki, T. Matsuzaki, H. Hagiwara, T. Aoki, and K. Takata, "Recent advances in fluorescent labeling techniques for fluorescence microscopy. acta histochem cytochem." *Acta Histochem Cytochem.*, pp. 131–137, 2007.

[10] A. Heindl, M. Schepelmann, R. Ecker, P. Pietschmann, I. Ellinger, A. Seewald, and T. Thalhammer, *Principles of Osteoimmunology: Molecular Mechanisms and Clinical Applications.* Springer, 2012.

[11] B. Filas, P. Bayly, and L. Taber, "Mechanical stress as a regulator of cytoskeletal contractility and nuclear shape in embryonic epithelia." *Ann Biomed Eng.*, pp. 443–454, 2010.

[12] E. Glazer, P. Bartels, A. Prasad, M. Yozwiak, H. Bartels, D. Einspahr, JG. Alberts, and R. Krouse, "Nuclear morphometry identifies a distinct aggressive cellular phenotype in cutaneous squamous cell carcinoma." *Cancer Prev Res (Phila).*, pp. 1770–1777, 2011.

[13] C. de Andrea, A. Petrilli, R. Jesus-Garcia, L. Bleggi-Torres, and M. Alves, "Large and round tumor nuclei in osteosarcoma: good clinical outcome." *Int J Clin Exp Pathol.*, pp. 169–174, 2011.

[14] S. Petushi, F. Garcia, M. Haber, C. Katsinis, and A. Tozeren, "Large-scale computations on histology images reveal grade-differentiating parameters for breast cancer." *BMC Med Imaging.*, 2006.

[15] V. Nandakumar, L. Kelbauskas, K. Hernandez, K. Lintecum, P. Senechal, K. Bussey, P. Davies, R. Johnson, and D. Meldrum, "Isotropic 3d nuclear morphometry of normal, fibrocystic and malignant breast epithelial cells reveals new structural alterations." *PLoS One.*, 2012.

[16] C. Chow and T. Kaneko, "Automatic boundary detection of the left ventricle from cineangiograms." *Comp. Biomed. Res.*, pp. 388–410, 1972.

[17] C. Yap and H. Lee, "Identification of cell nucleus using a mumford-shah ellipse detector." *Advances in Visual Computing Lecture Notes in Computer Science*, pp. 582–593, 2008.

[18] C. van Rijsbergen, *Information Retrieval (2nd ed.).* Butterworth, 1979.

[19] S. Kothari, Q. Chaudry, and W. MD., "A nonlinear mapping for data structure analysis," *IEEE Transactions on Computers*, pp. 401–409, 1969.

[20] M. Hall, E. Frank, G. Holmes, B. Pfahringer, P. Reutemann, and I. Witten, "The weka data mining software: An update." *SIGKDD Explorations*, 2009.

[21] D. Brllmann, A. Pabst, K. Lehmann, T. Ziebart, M. Klein, and B. d'Hoedt, "Counting touching cell nuclei using fast ellipse detection to assess in vitro cell characteristics: a feasibility study." *Clin Oral Investig.*, pp. 33–38, 2010.

[22] S. Kothari, Q. Chaudry, and W. MD., "Extraction of informative cell features by segmentation of densely clustered tissue images." *Conf Proc IEEE Eng Med Biol Soc.*, pp. 6706–6709, 2009.